Atmos. Chem. Phys. Discuss., 14, 30913–30945, 2014
www.atmos-chem-phys-discuss.net/14/30913/2014/
doi:10.5194/acpd-14-30913-2014

Atmospheric Chemistry and Physics Discussions

Examining the major contributors and controlling factors of ozone production in a rural area of the Yangtze River Delta region during harvest season

X. Pan[1], Y. Kanaya[2], H. Tanimoto[3], S. Inomata[3], Z. Wang[4], S. Kudo[3], and I. Uno[1]

[1]Research Institute for Applied Mechanics, Kyushu University, the work was done in Japan Agency for Marine-Earth Science and Technology, Japan
[2]Japan Agency for Marine-Earth Science and Technology, Japan
[3]National Institute for Environmental Studies, Japan
[4]State Key Laboratory of Atmospheric Boundary Layer Physics and Atmospheric Chemistry, Institute of Atmospheric Physics, Chinese Academy of Sciences, Japan

Received: 25 August 2014 – Accepted: 28 October 2014 – Published: 9 December 2014

Correspondence to: X. Pan (xlpanelf@riam.kyushu-u.ac.jp)

Published by Copernicus Publications on behalf of the European Geosciences Union.

Abstract

Open biomass burning (OBB) has been reported to emit substantial amounts of non-methane hydrocarbons (NMHCs), and the mixing of OBB with urban plumes could exacerbate regional ozone (O_3) pollution. In the present study, an observational field campaign was performed in a rural area at the edge of Yangtze River Delta region (YRDR) during harvest season when intensive open burning of wheat residues was observed. The O_3 production rate at the site was calculated using a photochemical box model (Regional Atmospheric Chemical Mechanism, Version 2) constrained by real-time ambient measurements (e.g., O_3, volatile organic compounds (VOCs), the sum of $NO_2 + NO$ (NO_x), J values). During the period impacted by OBB, the O_3 concentration frequently exceeded 100 ppbv. Analysis showed that the net O_3 production was pronounced, in particular when the site was characterized by a prevailing southerly wind that also brought substantial amounts of NO_x emitted from urban areas. At these times, the maximum rate of O_3 production was 20 ppbv h^{-1} with potential production rate of 102 ppbv on a daily basis. The O_3 production at the site was typically VOC-sensitive in the morning because NO_x dominated the plumes. However, in the afternoon, conditions became NO_x-sensitive due to the rapid photochemical consumption of NO_x in the production of O_3. A positive matrix factorization analysis indicated that solvent usage and OBB were the primary contributors to the mass fraction of ambient NMHCs observed at the study site, and were responsible for 35 and 23 % of the total O_3 production, respectively. The preferential presence of NO_x in the morning inhibited net O_3 production; meanwhile O_3 built up in the afternoon due to a decrease in NO_x concentrations. These results indicated that a joint effort in the regulation of solvent (aromatics) usage and OBB, as well as NO_x from on-road vehicle exhaust may be effective in eliminating high-O_3 pollution risk in the rural areas of the YRDR.

ACPD
14, 30913–30945, 2014

1 Introduction

Ozone (O_3) is a crucial component in the troposphere. It plays a key role in the atmosphere's oxidation capacity, which strongly influences the lifetime of biogenic/anthropogenic compounds and their corresponding climate forcing effects (Sitch et al., 2007). High concentrations of tropospheric O_3 has been reported to have serious detrimental environmental and health effects (e.g., crop yield reduction, human respiratory disorders) (Cape, 2008). In principle, the net production of O_3 is evident due to the presence of peroxy radicals from the photochemical oxidation of non-methane hydrocarbons (NMHCs), which significantly disturbs the O_3–NO–NO_2 cycle, especially in urban areas where atmospheric loadings of NMHCs and the sum of $NO_2 + NO$ (NO_x) are pronounced.

In China, the Yangtze River Delta region (YRDR) is one of the most important economic centers and is responsible for 11–12 % of total emission of NMHCs and NO_x in China (Zhang et al., 2009). These O_3 precursor emissions have increased by 71 % (NMHCs) and 89 % (NO_x) since 2000 (Kurokawa et al., 2013) due to rapid economic development in the region. Long-term observations have indicated that ground-level O_3 pollution in the YRDR has been increasing at a rate of $+0.52\,\mathrm{ppbv\,yr^{-1}}$ (Wang et al., 2009) and at a rate of $2.7\,\%\,\mathrm{yr^{-1}}$ in terms of variability in the daily maximum from 1991 to 2006 (Xu et al., 2008). Extreme O_3 pollution (hourly averages reaching 286 ppbv) has been reported at a suburban site near the Beijing megacity due to an abundance of local O_3 precursors (Wang et al., 2006).

Although open biomass burning (OBB) occurs sporadically and intensively, its impact on ambient O_3 levels has been shown to be statistically evident. Onboard satellite observations have indicated that troposphere column O_3 concentrations are enhanced by 10–25 % in near and downstream regions of fire (Ziemke et al., 2009). Such phenomena are supported by flight measurements (Takegawa et al., 2003) in which a clear positive correlation between O_3 and carbon monoxide (CO) measured in the OBB plume has been observed, implying that O_3 was photochemically produced from

ACPD
14, 30913–30945, 2014

its precursors emitted from OBB. A recent study found that methyl vinyl ketone (MVK) and methylacrolein (MACR) (photooxidation products of isoprene), as well as isoprene, are also present at significant levels in some OBB plumes, indicating that isoprene played essential role in the O_3 formation processes (Hornbrook et al., 2011). In China, large amounts of crop residue are burned directly in the field in harvest seasons, and such activities have remained intensive in the YRDR despite being legally banned by the government. The mixing of the OBB plume with anthropogenic pollutants (rich in NMHCs and NO_x) emitted from urban areas may significantly boost O_3 formation.

Recent analysis of the impact of OBB on regional O_3 production have generally been based on model simulations by manipulating the emissions of O_3 precursors from OBB, and results have been heavily dependent on the appropriateness and accuracy of OBB information (e.g., emission strength, geographical location, duration) (Yamaji et al., 2010). Quantitive analysis of the contribution of OBB to in situ O_3 production using field observations is still limited. In response to this limitation, a field measurement was carried out in a rural area of the YRDR from the middle of May to the end of June. The O_3 production rate and sensitivity were investigated using the Regional Atmospheric Chemistry Mechanism (RACM) version 2, which was constrained by real-time measurements of O_3 precursors, meteorological conditions, and J values. Positive matrix factorization (PMF) was adopted in this study to identify the possible sources of NMHCs at the site. Besides diagnosis of the O_3 production mechanism, this study also aimed to provide recommendations to policy-makers for effectively reducing the risk of high-O_3 pollution in the rural area of the YRDR.

2 Measurements

Field measurements of O_3, CO, NO_x, and NMHCs were carried out in a Science and Technology park in a rural area of the YRDR (32.25° N, 121.37° E; Rudong Town, Jiangsu Province, China) in June 2010. Local anthropogenic emissions in the Science and Technology park were very limited. The observation site was ~ 180 km north of

ACPD
14, 30913–30945, 2014

the Shanghai megacity, surrounded by acres of agriculture fields with few inhabitants. The geographic information for the observation site is shown in Fig. 1. In this study, the mixing ratio of O_3 was measured using a commercial UV-absorption O_3 analyzer (model 49c, time resolution: 1 min; zero noise: 0.25 ppbv with 1 min average; Thermo Scientific Inc.). The ambient CO mixing ratio was measured using a gas filter non-dispersive infrared carbon monoxide gas analyzer (model 48c, zero noise: 0.04 ppm with 30 s average; Thermo Scientific Inc.). The zero point was periodically checked during the beginning 20 min of each hour using purified air produced by a heated Pt catalyst (model 96; Thermo Electron Co.). Span calibrations were performed on site with standard span gas (2.03 ppmv, produced by Nissan-Tanaka Corp., Japan). Mixing ratios of NO and NO_2 were detected using a commercial NO_x analyzer (model 42CTL; Thermo Scientific Inc.). We used two converters in parallel that were switched from one to the other, a molybdenum converter for measurements of NO_y and a photolytic converter for selective measurements of NO_2. The precision of the instrument is specified to be 0.4 ppbv with a zero noise of 0.2 ppbv with a 1 min average. The instruments were placed in a temperature-controlled container and ambient air mass was drawn into the room through a 2.5 m-long, 1/4 inch Teflon tube.

Fifteen NMHCs species were detected using an online gas chromatography-flame ionization detection (GC-FID) and gas chromatography-mass spectrometry (GC-MS) at a time resolution of $\sim$ 2 h. During measurement, ambient air was first directed to a pre-concentration unit (GAS-30; DKK-TOA Corp., Ltd., Japan) with a sampling time of 10 min. Valves and transfer lines were maintained at 80 °C to minimize the loss of VOCs in samples, and the trapping tube was held at ~ -78 °C using liquid carbon dioxide. Calibration of the GC/FID/MS was carried out using a gas standard of 1 ppm containing 58 VOC components (PAMS-J58; Sumitomo Seika Chemicals Corp., Ltd., Japan). Oxygenated volatile organics (e.g., MVK/MCAR, MEK/butanal, acetone/propanal) and acetonitrile were also concurrently measured using a commercially available proton transfer reaction mass spectrometer (PTR-MS; Ionico Analytik GmbH, Austria). A detailed explanation of NMHC measurements is given in literature (Kudo et al., 2014). The

ACPD
14, 30913–30945, 2014

spectral actinic flux was measured using a single monochromator/photodiode array instrument (Meteorologie Consult Inc., Germany) with a wavelength ranging from 274 to 698 nm. The uncertainty in the photolysis of ozone (JO^1D) for a similar instrument has been estimated to be 14 %. Chemical composition and the size distribution of aerosol particles were also measured during the field campaign. Detailed descriptions of these methods can be found in the literature (Pan et al., 2012).

3 Methodologies

3.1 Observation-based simulation of O_3 production

The simulation of O_3 photochemistry was based on a photochemical box model, RACM, version 2, which was released recently (Goliff et al., 2013). Compared with its previous version (RACM version 1) (Stockwell et al., 1997), the new version has expanded aromatic chemistry with a greater number of species, and additional and separate reaction schemes for benzene, *m*-xylene, *p*-xylene, and *o*-xylene chemistry. This mechanism employs 363 reactions and 120 species. In the calculations, O_3, NO, NO_2, SO_2, CO, and J values, as well as NMHC species, were processed into a dataset with a time resolution of 10 min. The missing data were linearly interpolated. Concentrations of all species at 00:00 LST were regarded as the initial condition, and the integration was conducted repeatedly with an integration step of 0.01 s for five times on each day. Results of the last 24 h were used as the output of simulations after the stabilization of unmeasured species. The mixing ratio of NO was assumed to be 0.01 ppbv when the observation was below the detection limit. O_3 photochemistry in the daytime (06:00–18:00 LST) was manifested on the basis of the constrained steady-state calculation, and the instantaneous net O_x ($O_3 + NO_2$) production rate [$P(O_x)$] was also estimated since NO_2 is known to exist at high concentrations comparable to O_3 at the observation site. O_x net formation rate [$P(O_x)$] was calculated by subtracting its loss [$D(O_x)$] from

ACPD
14, 30913–30945, 2014

gross formation rate, $F(O_x)$. The formulae are given by

$$F(O_x) = k_1[HO_2][NO] + \sum k_{2i}[RO_2]_i[NO]\phi_i \quad (1)$$

$$D(O_x) = k_3[O^1(D)][H_2O] + k_4[OH][O_3] + k_5[HO_2][O_3] + \sum k_{6j}[O_3][\text{olefin}]_j + \sum k_7[OH][NO_2] \quad (2)$$

$$P(O_x) = F(O_x) - D(O_x) \quad (3)$$

where RO_2 and ϕ represent organic peroxy radicals (e.g., CH_3O_2) and the yield of NO_2 from the $RO_2 + NO$ reactions, [X] is the number density of species X, and k_1–k_7 are the reaction rate coefficients for the [X][Y] reaction. The calculation of $F(O_x)$, $D(O_x)$, and $P(O_x)$ depend on the final output of RACM simulations after the photochemical balance of peroxy radicals is achieved.

3.2 PMF analysis

Positive Matrix Factorization (PMF, version 5.0) is an advanced receptor model that analytically decomposes an $n \times m$ dimension matrix of observations into several factors (p), the species profile (f) of each source, and the amount of mass concentration (g) by solving a constrained and weighted least-squares optimization equation as follows:

$$x_{ij} = \sum_{k=1}^{p} g_{ik} f_{kj} + e_{ij} \quad (4)$$

where i and j represent the number of samples and chemical species that were measured, respectively, e_{ij} is the residual for each sample/species. The PMF solution minimizes the object function Q as follows:

$$Q = \sum_{i=1}^{n} \sum_{j=1}^{m} [e_{ij}/u_{ij}]^2 \quad (5)$$

ACPD
14, 30913–30945, 2014

Where u_{ij} is the uncertainty for each samples/species, the detailed description the model is in the user guide (http://www.epa.gov/heasd/research/pmf.html). This approach integrates non-negativity constraints into the computation to make the results physically meaningful and explainable. To avoid arbitrariness, the Q value was examined on the basis of theoretical calculations (Eq. 6) and the number of factor p, for which the PMF derived Q value nearest to the Q_{theory} value, was accepted as the numbers of NMHCs source:

$$Q_{\text{theory}} = m \times n - (m + n) \times p \quad (6)$$

In the PMF run, 1-butene, *trans*-2-butene, *cis*-2-butene, and isoprene were categorized as "weak" based on low signal-to-noise (S/N) ratios and their relatively strong photochemical activity. Final source appointment was determined on the basis of NMHCs tracers (such as alkane, aromatics, and acetonitrile). Bootstrap runs with 100 random seed were tested. Scatterplots of different factors generally filled the G-space, and F-peak calculations also showed very similar results, implying that the PMF calculation was reliable for use in the following analysis.

3.3 Footprint analysis

An ensemble simulation of a 72 h back trajectory of air masses was performed using the Hybrid Single Particle Lagrangian Integrated Trajectory model (Hysplit; http://ready.arl.noaa.gov/HYSPLIT.php) by offsetting the meteorological data by a single meteorological grid point in the horizontal and 0.01 sigma units in the vertical. Input meteorological data were provided by the NCEP Global Data Assimilation System (GDAS) model with a grid resolution of $1^\circ \times 1^\circ$. To better review the impact of emissions on the surface layer, only the footprint region of the air mass in units of residence time was demonstrated in the following analysis. Here, the footprint region was determined as the grids in which the geographical height of the trajectory point was lower than the mixing height in the meteorological field. The footprint region was generally consistent with

ACPD
14, 30913–30945, 2014

the spatial distribution of source–receptor relationships determined by the FLEXPART dispersive model (Pan et al., 2012).

4 Results

4.1 Overview of observations

Temporal variations in the O_3, NMHC, NO_x, NO_y, and CO mixing ratios are shown in Fig. 2, and statistics on the NMHC species are listed in Table 1. During observation periods, five pollution episodes (10–12 June, 14–17 June, 18–20 June, 22 June, and 23 June) were clearly observed on the basis of NO_x variations, and on 4 days (15 June, 19 June, 22 June, and 23 June), the hourly averaged O_3 mixing ratio had maxima greater than 100 ppbv (dash line as shown in the Fig. 2). The highest O_3 concentration (147 ppbv) occurred on 15 June when the site was affected by the intensive open burning of crop residues in the surrounding agriculture area, and the daily averaged CO mixing ratio was found to be 1000 ppbv. During high pollution periods, the significant increase in O_3 during the daytime at the site was mainly related to the O_3 precursors transported from the megacity cluster to the south, illustrated by the obvious enhancements in NO_x (mean: 30 ppbv) and NO_y (mean: 60 ppbv) observed with the prevailing southerly wind. In particular, the ambient O_3 mixing ratio decreased to almost zero due to titration reactions when the nitrogenous species were present in the early morning of pollution days. The ambient NMHC concentration was found to be 200 ppbC on average, and the maximum concentration of NMHCs (451 ppbC) occurred at 05:00 LST on 19 June when the NO_x mixing ratio was as high as 30 ppbv, and the maximum O_3 level also exceeded 120 ppbv due to strongly photochemical processes in the daytime. NMHCs showed a similar variation to CO, implying that they likely originated from the same sources during the field campaign. Note that the field campaign was just within the period of Shanghai World Expo 2010 with increased traffic and visitors. The local governments of Shanghai and Jiangsu Province implemented strict emissions control

ACPD
14, 30913–30945, 2014

operations including odd-and-even license plate rules for cars on the road, confining the assembly line of spraying treatment in auto-repair and industry enterprises, and prohibiting, e.g., OBB activities. Atmospheric O_3 precursors might have been even higher than this observation if no relevant regulatory measures had been in effect.

4.2 Diurnal pattern

Figure 3 shows the average diurnal variations in O_x, CO, NO, NO_x, NO_y, NO_z, NO_x/NO_y, and NMHCs for days when the maximum hourly averaged O_x concentration was greater than 100 ppbv (red dotted lines) and those days when it was less than 100 ppbv (blue dotted lines). The hourly averaged O_x in high-O_3 pollution days showed a predominant single peak distribution with a daily increment of 94 ppbv (Fig. 3a), suggesting the significant depletion of O_3 at night and production of O_3 in the daytime due to the presence of substantial concentrations of O_3 precursors. In contrast, O_x levels on the low-O_3 pollution days showed a moderate increase at noontime with a daily increment of 24 ppbv. Variation in NO (Fig. 3b) had a prominent peak at 07:00 LST, especially for the high-O_3 pollution days (maximum: 4.2 ppbv). For the low-O_3 pollution days, the hourly averaged NO normally had a weak peak (1.1 ppbv). As shown by the red line in Fig. 3c, diurnal variation in NO_2 at the site had a predominant peak (38.6 ppbv) between 00:00 and 08:00 LST, evidently different from the features (two peaks at 09:00 and 18:00 LST during rush hour) observed at the urban site of the Shanghai megacity. These results suggested that NO_2 at the site could be primarily attributable to transport from the urban area instead of in situ production. Diurnal variation in NO_y (Fig. 3d) on high-O_3 pollution days showed a boarder peak (57 ppbv) than that of NO_2 due to the consecutive conversion from NO_x to NOz (e.g., HNO_3, PANs) in the daytime. As expected, NO_z also showed an obviously unimodal distribution (Fig. 3e) with a maximum value of 32.6 ppbv at 12:00 LST when O_3 photochemistry was proactive. We did not observe a clear increase in either NO_y or NO_z for the low-O_3 pollution days.

ACPD
14, 30913–30945, 2014

Diurnal variation in the NO_x/NO_y ratio is illustrated in Fig. 3f. In general, a higher NO_x/NO_y ratio indicates that pollution plumes have a shorter photochemical age. In the present study, we found that the plumes on high-O_3 pollution days were not photochemically aged (NO_x/NO_y ratio > 0.5) when they were transported to the observation site in the morning, and they gradually became aged (NO_x/NO_y = 0.2) due to strong photochemical processes in the daytime. For low-O_3 pollution days, the NO_x/NO_y ratio did not vary significantly and had a mean of 0.34.

As shown in Fig. 3g, the total NMHC concentration (not including oxygenated VOCs) on the high-O_3 pollution days showed evident increases in the early morning (mean: 176.4 ppbC) and gradually decreased to 48.7 ppbC at night. On low-O_3 pollution days, the NMHC concentration was constantly low with a mean of 62.8 ppbC, implying limited contribution from the transport of urban emissions. Diurnal variations in J (NO_2) on the high-O_3 and low-O_3 pollution days during observation periods (Fig. 3h) showed nearly the same behavior, implying that the significant enhancement of O_3 production during the high-O_3 pollution period did not result from variations in solar radiation.

4.3 Identification of source regions

To identify the major source regions for O_3 precursors, the color-shaded polar graph for O_3, NO, NO_2, NMHCs, NO_x/NO_y and NMHC/NO_x is shown in Fig. 4. Figure 4a indicates that a weak southerly wind ($\sim 3\,m\,s^{-1}$) was mostly accompanied by the occurrence of high-O_3 pollution at the site, suggesting that in situ photochemistry was important in O_3 production; however, the high-O_3 concentration from the north and east was normally related with stronger winds ($> 5\,m\,s^{-1}$), implying the potential contribution from direct transport. As expected, high NO_x (Fig. 4b and c) and NHMCs (Fig. 4d) at the site were also related to prevailing southerly winds that brought substantial amounts of O_3 precursors from the megacity cluster (e.g., Shanghai). Figure 4e shows that polluted plumes from the west and south were normally fresh with an NO_x/NO_y ratio larger than

ACPD
14, 30913–30945, 2014

0.5, especially during the high-O_3 pollution days when the NO_x/NO_y ratio was greater than 0.8.

The NMHC/NO_x ratio partially reflected the characteristics of emissions sources and corresponding O_3 production potentials. The dependence of NMHC/NO_x on wind direction is shown in Fig. 4f. We found that the polluted plumes from the north normally had high NMHC/NO_x ratios with a mean of 41 ppbC ppb^{-1}. Nevertheless, typically low NMHC/NO_x ratios (12 ppbC ppb^{-1} on average) were observed in the present study for plumes transported from the metropolis to the south. Ran et al. (2009) reported an average NMHC/NO_x ratio of 8 ppbC ppb^{-1} for pollution in the downtown area of the Shanghai megacity, generally consistent with our observations. For a detailed discussion on the dependence of O_3 production on the NMHC/NO_x ratio, see Sect. 5.3.

5 Discussions

5.1 O_3 production rate

The net photochemical production of O_3 [$P(O_3)$] during the field campaign was calculated on the basis of Eqs. (1)–(3). In general, the buildup of O_3 pollution at the site could be mostly explained by the instantaneous photochemical production rate assessed by the box model constrained by local observations of precursors. Figure 5 shows the diurnal variation in $P(O_3)$ for high-O_3 pollution days and the entire observation period. For the high-O_3 pollution days, the maximum $P(O_3)$ was 20.1 ppbv h^{-1} at 11:00 LST. The 6 h (09:00–15:00 LST) average of $P(O_3)$ was found to be 13.3 ppbv h^{-1}, which is similar to the 6 h averages found from observations over other urban areas (Philadelphia, PA: 11.3 ppbv h^{-1}; Houston, TX: 11.3 ppb h^{-1}) (Kleinman et al., 2002). The observation was higher than results at the top of Mt.Tai (1534 m) in Central East China (6.4 ppbv h^{-1}) where O_3 production has been found to be primarily NO_x-limited (Kanaya et al., 2009). Daily integrated $P(O_3)$ levels on high-O_3 and low-O_3 days were 102 and 34 ppbv, respectively. These amounts were larger than the observed increase of O_3 concentration

ACPD
14, 30913–30945, 2014

(93 and 24 ppbv, respectively) in the daytime, implying that a buildup of O_3 at Rudong could be generally explained by in situ photochemical productions, without taking into account import of O_3 produced in other areas. One exception was 22 June when the $P(O_3)$ (17 ppbv) accounted for only one-tenth of the observed O_3 production (151 ppbv) on a daily basis, suggesting that the direct transport of O_3 was more important for the enhancement of O_3 mixing ratio observed at the site. Footprint analysis implied that the contribution from the Shanghai megacity was significant.

5.2 Dependence of O_3 production sensitivity on the source region

The sensitivity of O_3 production to precursor concentrations was determined on the basis of model simulations by artificially multiplying the NO_x concentration by factors of 0.5 and 2, while the NMHC concentration was kept unchanged, or by multiplying the NMHC concentration by factor of 0.5 and 2, while the NO_x concentration remained unchanged. The sensitivity of the O_3 production rate on several O_3 pollution cases and their corresponding footprint regions was determined by a back trajectory model (Fig. 6). As shown in Fig. 4, the emission characteristics of O_3 precursors observed at the observation site differed for pollutants arising from different directions, resulting in specific O_3 production sensitivity. For the pollution that originated from the western inland area (Fig. 6a and b), O_3 production was very sensitive to the variation in VOCs, and a decrease in NO_x led to an obvious increase in O_3 production, even in the afternoon when NO_x had been significantly consumed, which suggested that O_3 production occurred in a typically VOC-controlled regime. However, when the air masses originated from the north/coastal region (Fig. 6d), O_3 production was primarily controlled by ambient NO_x concentrations (Fig. 6c), as indicated by the extremely low NO_x concentration (average: 0.93 ppbv) and relatively high NMHC concentration (42.5 ppbv) in the daytime.

Most notably, we observed an obvious alteration in O_3 production sensitivity for the pollution transported from the south region (Fig. 6e–h). O_3 production in the morning was much more sensitive to the NMHC concentration than to NO_x, and an increase in

ACPD
14, 30913–30945, 2014

NO_x concentration resulted in a decrease in O_3 production (VOC-controlled regime); in the afternoon, the O_3 production became NO_x-sensitive and a doubling of the NO_x concentration led to a clear increase in O_3 production (NO_x-controlling regime). This reflected significant variations in ambient NO_x due to photochemical processes in the atmosphere, and the NO_x mixing ratio decreased from 21.7 ppbv in the morning to 2.9 ppbv in the afternoon on 19 June and from 39.4 to 2.0 ppbv on 23 June. Footprint analysis (Fig. 6f and h) indicated that the air mass was mostly stagnant over polluted regions in the YRDR, implying that anthropogenic pollution (e.g., automotive vehicles) from urban areas was a determinant in the variation in O_3 production.

5.3 O_3 production isopleth diagram

To better evaluate the O_3 production sensitivity to NMHCs and NO_x concentrations at the site, a series of model runs were carried out that artificially decreased and increased the NO_x and NMHC concentration to cover wide areas to simulate real atmospheric conditions as described in Sect. 5.2. The mixing ratio of O_3, NO_x, and NMHCs, J values, and meteorological data observed at 10:00 LST on 19 June were used as constraints. The dependence of the O_3 production rate on NMHCs and NO_x is shown in Fig. 7. The circles and squares in the plot represent the calculated O_3 production rate observed on high-O_3 pollution days (19 and 23 June), and the gray dashed lines indicate a variation in NO_x during those days. The shift in the O_3 production regime on high-O_3 pollution days could be explained by the diagram. The model predicted that the ridge of the O_3 production rate was associated with an NMHC/NO_x ratio of 10–20 ppbC ppbv^{-1}, similar to the prediction of urban photochemistry in central Tokyo (Kanaya et al., 2008). Relatively low NMHC/NO_x ratios ($\sim$ 5 ppbC ppbv^{-1}) were found in the mornings of high-O_3 pollution days owed to a substantial amount of NO_x, which increased slightly up to 30–50 ppbC ppbv^{-1} due to rapid NO_x photochemical loss. This tendency was generally consistent with the observation in Shanghai urban area (Ran et al., 2009).

ACPD
14, 30913–30945, 2014

In particular, O_3 production in the morning of 19 June approached the predicted "ridge" region due to the preferential presence of hydroperoxyl (HO_2) and peroxy radials on the basis of model calculations, and the pathway forming NO_2 by peroxy radials reacting with NO was predominant. Footprint analysis illustrated that the accumulation of NMHCs in air masses was associated with urban emissions north of the YRDR. The difference was that O_3 production in the morning of 23 June occurred in a typical NO_x-inhibition regime due to the extremely low NMHC/NO_x ratio (1.1 ppbC ppbv^{-1}). The footprint of air masses demonstrated a clear "U"-shape where the air masses were mostly transported from marine region and swept over the Shanghai megacity. As mentioned before, the field campaign was performed during the Shanghai Expo period. A reduction of NO_x and NMHC emissions in the YRDR due to regulatory emission policies likely inhibited O_3 production; however it did not appear to change the primary conclusion of O_3 production sensitivity at this site, especially since the site was situated downwind of the polluted urban areas.

5.4 Contribution of O_3 production from different sources

5.4.1 Allocation of anthropogenic NMHC sources

Source appointment of NMHCs observed during the field campaign was performed on the basis of PMF calculation, and six anthropogenic sources were mathematically resolved. Factor 1 explained most of the aromatic mass fraction with 79 % for toluene, 88 % for ethyl-benzene, 79 % for *m*, *p*-xylene, and 75 % for *o*-xylene. Alkane and alkene accounted for only a minor percentage of the total mass, suggesting that this factor was primarily associated with solvent use sources. Mass ratios of *m*, *p*-xylene/*o*-xylene (1.4) were found to be similar to the values reported for painting factories (2.0) and the solvent-based industry (2.2) around the Shanghai megacity (Cai et al., 2010).

Factor 2 was regarded as OBB sources due to the predominant contribution of furan and acetonitrile to this factor with mass fractions of 70 and 39 %, respectively. We found that OBB could explain 74.4 % of total isoprene and 55.4 % of the MVK + MACR (oxi-

ACPD
14, 30913–30945, 2014

dation production of isoprene) at the study site. This result was slightly higher than the value in the emissions inventory, which indicated that 54.3 % of isoprene in the YRDR originated from biomass burning (Huang et al., 2011). We found that the furan/isoprene mass ratio in OBB was 16.2, much higher than the value (3.5) reported in the emissions inventory (Akagi et al., 2011) and higher than the value (2.6) observed in laboratory experiments (Christian et al., 2003). The higher ratio in the present study was probably due to the photo-oxidation of isoprene in the summer season, and the furan/isoprene ratio would be approximately equal to that of previous studies if MVK/MACR were taken into consideration. Note that the isoprene from biogenic sources was negligible compared to the contribution from OBB and anthropogenic emissions during these specific observation episodes (Sect. 5.4.3).

Factor 3 explained the majority of C_5 alkane mass representing 69 % of *i*-pentane and 70 % of *n*-pentane. *i*-pentane is a typical tracer for gasoline evaporation, and we therefore assigned this factor to fuel evaporation sources. Factor 4 accounted for 54 and 78 % of the total mass of *i*-butane and *n*-butane, respectively, the latter of which is reportedly released from the use of liquid petroleum gas (LPG) and natural gas (NG), which are the major fuels consumed for household cooking in the YRDR. We then attributed this factor to domestic sources related with LPG usage. Factor 5 was assigned to vehicular-exhaust sources due to a predominance of NO_2 (77 %), which was reported to be the characteristic product of the internal combustion of fossil fuel. Quantities of aromatics and alkane species in this factor were small. Factor 6 was attributed to the oil industry (such as petroleum refining) due to a significant contribution of propane (one of the major by-products of raw oil processing) and benzene (a petrol additive), accounting for 84 and 55 %, respectively.

5.4.2 Diurnal variation in the factorial contribution to O_3 production

The sensitivity of each source to O_3 production at the study site is quantified in this section. First, the NMHC and NO_x concentrations of one selected source were artificially increased/decreased by 10 % while the concentration of NMHCs and NO_x for

ACPD
14, 30913–30945, 2014

other sources remained unchanged. In such a situation, the total variation in NMHC and NO_x concentrations was normally within 5 %, guaranteeing that the RACM2 calculation could still be well constrained. The variation in O_3 production rates that resulted from chemical reactions was deemed as the relative contribution of the source to O_3 formation. Average diurnal variation in the relative sensitivity of six sources to in situ photochemical O_3 formation is shown in Fig. 8. The contribution of different sources to O_3 production demonstrated distinct variation patterns. Solvent usage was responsible for major contributions (52 %) of O_3 production in the morning and minor contributions (18 %) in the afternoon. The second most important contributor was OBB with a maximum contribution of 27 % at 12:00 LST and 23 % on a daily basis. These results imply that the regulation of OBB in the rural area of the YRDR is definitely effective in reducing the potential risk of high-O_3 pollution, although these effects may differ from region to region. Industrial sectors contributed 31 % of the total O_3 formation in the afternoon. In particular, the increase in vehicle exhaust-related sources tended to depress the formation of O_3 in the morning because the air mass was rich in fresh NO_x (typical VOCs-sensitive regime); however, in the afternoon, vehicle exhaust can boost the production of O_3 due to NO_x-sensitive atmospheric state (as discussed in Sect. 5.3). The vehicle exhaust-related source was responsible for 16 % of the O_3 production in the afternoon. In general, the total sensitivity of each source could explain most of the variability in O_3 production rates at the site (Fig. 5).

5.4.3 Biogenic isoprene

In the present study, mean mass concentrations of isoprene and MVK/MACR (photooxidation products of isoprene) at the site were 0.16 ± 0.15 ppbv and 0.83 ± 0.55 ppb, respectively, with a mean MVK + MACR to isoprene ratio ([MVK + MACR]/isoprene) of 5.2. Biogenic sources (normally predominant at noon) were not mathematically resolved by the PMF calculation. Most of the isoprene was attributed to OBB sources and the rest was assigned to sources related to transport. First, the [MVK + MACR]/isoprene ratio was normally less than 0.4 in the biogenic sources-dominant

ACPD
14, 30913–30945, 2014

environment (Montzka et al., 1993). Yuan et al. (2012) reported that the [MVK + MACR]/isoprene ratio was 0.3 for biogenic sources on the basis of PMF analysis. In the present study, the [MVK + MACR]/isoprene ratio was the highest, ranging from 3 to 25, suggesting that the impact of biogenic sources was not significant. Second, oxygenated VOCs (including MVK and MACR) might also be preferentially present in the OBB plumes, and the [MVK + MACR]/isoprene ratio was reported as ranging from 1.8 to 4.2 in the emissions inventory (Akagi et al., 2011). The relatively higher [MVK + MACR]/isoprene mass ratio in the present study implied that the isoprene might undergo further oxidization after being emitted. The upper limit of the [MVK + MACR]/isoprene ratio was ~ 30 in this study. Third, observation site was located adjacent to a large area of wheat field, it is known that wheat plants emit little amount of isoprene (Kesselmeier and Staudt, 1999), the diurnal variation in isoprene at the site did not show a pronounced enhancement at noontime (10:00–15:00 LST), and the 6 h averaged isoprene concentration was 0.19 ± 0.16 ppbv. Given the above, we deemed that biogenic sources had limited impact on in situ O_3 production and was therefore neglected in the above discussion.

5.4.4 Impact of aerosols on O_3 production

The presence of particles reportedly can result in a significant heterogeneous loss of HO_2 (Taketani et al., 2008), which plays a key role in peroxy radical equilibrium and O_3 formation in the troposphere. The study at the mountain site in Central East China indicated that ambient HO_2 concentrations, and corresponding net O_3 production rates, declined significantly, due to the inclusion of a heterogeneous loss in HO_2 (Kanaya et al., 2009). In the present study, the effect of a heterogeneous loss of HO_2 on the O_3 production rate was investigated. The loss rate of HO_2 was calculated using the Fuchs–Sutugin equation (refers to the paper, Kanaya et al., 2009). The gas-phase diffusion coefficient of HO_2 was assumed to be 0.247 $cm^2 s^{-1}$. The dependence of the uptake coefficient of HO_2 on relative humidity (ranging from 0.2 to 0.35) was considered on the basis of laboratory studies (Taketani et al., 2008). The number size distribution of par-

ACPD
14, 30913–30945, 2014

ticles (size bins: 0.3–0.5, 0.5–0.7, 0.7–1.0, 1.0–2.0, 2.0–5.0 µm) during the campaign were measured using a portable particle counter (model KR-12A; RION Inc.). As a result, the estimated loss rate of HO_2 ranged from 7×10^{-3} to $0.05\,s^{-1}$. The incorporation effect of HO_2 loss into the RACM2 model calculation resulted in the O_3 production rate being reduced by 13 % on average; however, it was still large enough to explain the buildup of O_3 at the site. Note that emissions of $PM_{2.5}$ and ambient concentrations in the East China region have been increasing for the past decades due to rapid economic growth. Huang et al. (2011) reported that primary anthropogenic emissions of $PM_{2.5}$ and PM_{10} in the YRDR were $1510.8\,Gg\,yr^{-1}$ and $3115.7\,Gg\,yr^{-1}$, respectively, correspondingly accounting for 11 and 17 % of the total emissions in China. O_3 production was inferred to have been depressed due to the presence of a substantial number of aerosol particles (heterogeneous loss of HO_2) in the atmosphere, and tropospheric O_3 concentrations were assumed to definitely increase provided that particle emissions are significantly reduced while NO_x and NMHCs emission remain unchanged. Furthermore, a reduction in fine particle concentrations in atmosphere will also decrease the aerosol optical depth, resulting in an increase in the actinic flux and photolysis rates in the lower troposphere. A study by (Gerasopoulos et al., 2013) found a 40 % reduction in JO^1D at a high solar zenith angle during high aerosol loading periods (AOD = 0.5–0.7), implying that the enhancement of O_3 production will more drastic if the effects of both a reduction of heterogeneous loss and an increase in J values were considered. Moreover, the variability in meteorological conditions should also impact O_3 production. For example, an increase in relative humidity could lead to a more rapid heterogeneous loss of HO_2 on the wet surface of particles (Taketani et al., 2008). To summarize, including the impact of aerosols is extremely important in reviewing and predicting O_3 pollution in East Asia under the scenario of global warming.

ACPD
14, 30913–30945, 2014

6 Conclusion and implications

This study synthesized field observations in a rural area of the YRDR during harvest season. A photochemical box model (RACM version 2) was used to investigate the O_3 production rate, controlling regime and its possible contributors. These results demonstrated that O_3 pollution was serious, especially when the site was subject to the OBB plumes and urban pollutions transported from megacities (e.g., Shanghai). The hourly mixing ratios of O_3 and NMHCs on high-O_3 pollution days (hourly averaged O_3 mixing ratio > 100 ppbv) were 138 ppbv and 451 ppbC, respectively, almost the highest values reported in this region among previous studies. On high-O_3 pollution days, the diurnal variation in O_3 production rates had a maximum value of 20.1 ppbv h^{-1} and a daily-accumulated O_3 production rate of 102 ppbv, suggesting that in situ photochemical production could explain most of the O_3 buildup at the site. When pollution came from the Shanghai megacity with southerly winds, O_3 production sensitivity at the site was NMHC-controlled in the morning, but changed to NO_x-controlled in the afternoon due to a significant depletion of NO_x. PMF analysis indicated that six anthropogenic sources (solvent usage, OBB, fuel evaporation, liquid petroleum usage, vehicle exhaust, and the oil industry) contributed to the NMHC species observed at the site. Among these sources, solvent usage and OBB were the two most important contributors to high-O_3 concentrations, accounting for 35 and 23 %, respectively, of the O_3 production on a daily basis, followed by the oil industry (21 %). Vehicular exhaust sources were mostly responsible for the net production of O_3 in the afternoon, which was NO_x-sensitive. Biogenic isoprene emissions were found to be less important to the O_3 production at the site during our study period. Our results imply that the regulation of solvent usage and OBB in the YRDR are optimal measures to reduce the risk of high-O_3 pollution events. Meanwhile a reduction in NO_x emission from on-road transport seemed also to be effective in mitigating O_3 production in the daytime.

Acknowledgements. The authors thank the staff of the Rudong Municipal Environment Protection Bureau who provided us with assistance and facilitated the preparation and implementation

ACPD
14, 30913–30945, 2014

of the field campaign. This work was supported by the Environment Research and Technology Development Fund (S-7, C-081, B-051) from the Ministry of the Environment, Japan.

References

Akagi, S. K., Yokelson, R. J., Wiedinmyer, C., Alvarado, M. J., Reid, J. S., Karl, T., Crounse, J. D., and Wennberg, P. O.: Emission factors for open and domestic biomass burning for use in atmospheric models, Atmos. Chem. Phys., 11, 4039–4072, doi:10.5194/acp-11-4039-2011, 2011.

Cai, C. J., Geng, F. H., Tie, X. X., Yu, Q. O., and An, J. L.: Characteristics and source apportionment of VOCs measured in Shanghai, China, Atmos. Environ., 44, 5005–5014, 2010.

Cape, J.: Surface ozone concentrations and ecosystem health: past trends and a guide to future projections, Sci. Total Environ., 400, 257–269, 2008.

Christian, T., Kleiss, B., Yokelson, R., Holzinger, R., Crutzen, P., Hao, W., Saharjo, B., Ward, D.: Comprehensive laboratory measurements of biomass-burning emissions: 1. Emissions from Indonesian, African, and other fuels, J. Geophys. Res.-Atmos., (1984–2012), 108, doi:10.1029/2003JD003704, 2003.

Gerasopoulos, E., Mihalopoulos, N., Kazadzis, S., Vrekoussis, M., Liakakou, E., Kouvarakis, G., Kouremeti, N.: Factors controlling the variability of photolysis rates of NO_2 and O^1D in the complex environment of the Eastern Mediterranean, Advances in Meteorology, Clim. Atmos. Phys., Springer, 975–980, 2013.

Goliff, W. S., Stockwell, W. R., and Lawson, C. V.: The regional atmospheric chemistry mechanism, version 2, Atmos. Environ., 68, 174–185, 2013.

Hornbrook, R. S., Blake, D. R., Diskin, G. S., Fried, A., Fuelberg, H. E., Meinardi, S., Mikoviny, T., Richter, D., Sachse, G. W., Vay, S. A., Walega, J., Weibring, P., Weinheimer, A. J., Wiedinmyer, C., Wisthaler, A., Hills, A., Riemer, D. D., and Apel, E. C.: Observations of nonmethane organic compounds during ARCTAS – Part 1: Biomass burning emissions and plume enhancements, Atmos. Chem. Phys., 11, 11103–11130, doi:10.5194/acp-11-11103-2011, 2011.

Huang, C., Chen, C. H., Li, L., Cheng, Z., Wang, H. L., Huang, H. Y., Streets, D. G., Wang, Y. J., Zhang, G. F., and Chen, Y. R.: Emission inventory of anthropogenic air pollutants and VOC

ACPD
14, 30913–30945, 2014

species in the Yangtze River Delta region, China, Atmos. Chem. Phys., 11, 4105–4120, doi:10.5194/acp-11-4105-2011, 2011.
Kanaya, Y., Fukuda, M., Akimoto, H., Takegawa, N., Komazaki, Y., Yokouchi, Y., Koike, M., and Kondo, Y.: Urban photochemistry in central Tokyo: 2. Rates and regimes of oxidant ($O_3 + NO_2$) production, J. Geophys. Res., 113, D06301, doi:10.1029/2007JD008671, 2008.
Kanaya, Y., Pochanart, P., Liu, Y., Li, J., Tanimoto, H., Kato, S., Suthawaree, J., Inomata, S., Taketani, F., Okuzawa, K., Kawamura, K., Akimoto, H., and Wang, Z. F.: Rates and regimes of photochemical ozone production over Central East China in June 2006: a box model analysis using comprehensive measurements of ozone precursors, Atmos. Chem. Phys., 9, 7711–7723, doi:10.5194/acp-9-7711-2009, 2009.
Kesselmeier, J. and Staudt, M.: Biogenic volatile organic compounds (VOC): an overview on emission, physiology and ecology, J. Atmos. Chem., 33, 23–88, 1999.
Kleinman, L. I., Daum, P. H., Imre, D., Lee, Y. N., Nunnermacker, L. J., Springston, S. R., Weinstein Lloyd, J., and Rudolph, J.: Ozone production rate and hydrocarbon reactivity in 5 urban areas: A cause of high ozone concentration in Houston, Geophys. Res. Lett., 29, 1–4, 2002.
Kudo, S., Tanimoto, H., Inomata, S., Saito, S., Pan, X., Kanaya, Y., Taketani, F., Wang, Z., Chen, H., Dong, H., Zhang, M., and Yamaji, K.: Emissions of nonmethane volatile organic compounds from open crop residue burning in the Yangtze River Delta region, China, J. Geophys. Res.-Atmos., 119, doi:10.1002/2013JD021044, 2014.
Kurokawa, J., Ohara, T., Morikawa, T., Hanayama, S., Janssens-Maenhout, G., Fukui, T., Kawashima, K., and Akimoto, H.: Emissions of air pollutants and greenhouse gases over Asian regions during 2000–2008: Regional Emission inventory in ASia (REAS) version 2, Atmos. Chem. Phys., 13, 11019–11058, doi:10.5194/acp-13-11019-2013, 2013.
Montzka, S. A., Trainer, M., Goldan, P. D., Kuster, W. C., and Fehsenfeld, F. C.: Isoprene and its oxidation-products, methyl vinyl ketone and methacrolein, in the rural troposphere, J. Geophys. Res.-Atmos., 98, 1101–1111, 1993.
Pan, X., Kanaya, Y., Wang, Z., Taketani, F., Tanimoto, H., Irie, H., Takashima, H., and Inomata, S.: Emission ratio of carbonaceous aerosols observed near crop residual burning sources in a rural area of the Yangtze River Delta Region, China, J. Geophys. Res.-Atmos., (1984–2012), 117, doi:10.1029/2012JD018357, 2012.
Ran, L., Zhao, C., Geng, F., Tie, X., Tang, X., Peng, L., Zhou, G., Yu, Q., Xu, J., and Guenther, A.: Ozone photochemical production in urban Shanghai, China: Analy-

ACPD
14, 30913–30945, 2014

sis based on ground level observations, J. Geophys. Res.-Atmos., (1984–2012), 114, doi:10.1029/2008JD010752, 2009.
Sitch, S., Cox, P., Collins, W., and Huntingford, C.: Indirect radiative forcing of climate change through ozone effects on the land-carbon sink, Nature, 448, 791–794, 2007.
Stockwell, W. R., Kirchner, F., Kuhn, M., and Seefeld, S.: A new mechanism for regional atmospheric chemistry modeling, J. Geophys. Res., 102, 25847–25879, 1997.
Takegawa, N., Kondo, Y., Ko, M., Koike, M., Kita, K., Blake, D., Hu, W., Scott, C., Kawakami, S., and Miyazaki, Y.: Photochemical production of O_3 in biomass burning plumes in the boundary layer over northern Australia, Geophys. Res. Lett., 30, doi:10.1029/2003GL017017, 2003.
Taketani, F., Kanaya, Y., and Akimoto, H.: Kinetics of heterogeneous reactions of HO_2 radical at ambient concentration levels with $(NH_4)_2SO_4$ and NaCl aerosol particles, J. Phys. Chem. A, 112, 2370–7, 2008.
Wang, T., Ding, A., Gao, J., and Wu, W. S.: Strong ozone production in urban plumes from Beijing, China, Geophys. Res. Lett., 33, doi:10.1029/2006GL027689, 2006.
Wang, T., Wei, X. L., Ding, A. J., Poon, C. N., Lam, K. S., Li, Y. S., Chan, L. Y., and Anson, M.: Increasing surface ozone concentrations in the background atmosphere of Southern China, 1994–2007, Atmos. Chem. Phys., 9, 6217–6227, doi:10.5194/acp-9-6217-2009, 2009.
Xu, X., Lin, W., Wang, T., Yan, P., Tang, J., Meng, Z., and Wang, Y.: Long-term trend of surface ozone at a regional background station in eastern China 1991–2006: enhanced variability, Atmos. Chem. Phys., 8, 2595–2607, doi:10.5194/acp-8-2595-2008, 2008.
Yamaji, K., Li, J., Uno, I., Kanaya, Y., Irie, H., Takigawa, M., Komazaki, Y., Pochanart, P., Liu, Y., Tanimoto, H., Ohara, T., Yan, X., Wang, Z., and Akimoto, H.: Impact of open crop residual burning on air quality over Central Eastern China during the Mount Tai Experiment 2006 (MTX2006), Atmos. Chem. Phys., 10, 7353–7368, doi:10.5194/acp-10-7353-2010, 2010.
Yuan, B., Shao, M., Gouw, J., Parrish, D. D., Lu, S., Wang, M., Zeng, L., Zhang, Q., Song, Y., Zhang, J.: Volatile organic compounds (VOCs) in urban air: How chemistry affects the interpretation of positive matrix factorization (PMF) analysis, J. Geophys. Res.-Atmos., (1984–2012), 117, doi:10.1029/2012JD018236, 2012.
Zhang, Q., Streets, D. G., Carmichael, G. R., He, K. B., Huo, H., Kannari, A., Klimont, Z., Park, I. S., Reddy, S., Fu, J. S., Chen, D., Duan, L., Lei, Y., Wang, L. T., and Yao, Z. L.: Asian emissions in 2006 for the NASA INTEX-B mission, Atmos. Chem. Phys., 9, 5131–5153, doi:10.5194/acp-9-5131-2009, 2009.

ACPD
14, 30913–30945, 2014

Ziemke, J., Chandra, S., Duncan, B., Schoeberl, M., Torres, O., Damon, M., and Bhartia, P.: Recent biomass burning in the tropics and related changes in tropospheric ozone, Geophys. Res. Lett., 36, doi:10.1029/2009GL039303, 2009.

ACPD
14, 30913–30945, 2014

Table 1. Statistics on the mixing ratios of NMVOC species, NO_2, and black carbon (BC) during the field campaign.

Species	Average	SD	Median	10th percentile	90th percentile
Propane	1.23	2.23	0.54	0.14	2.47
Propylene	0.71	1.49	0.24	0.08	1.39
i-Butane	0.85	1.11	0.39	0.12	2.19
n-Butane	1.31	1.62	0.72	0.11	3.57
t-2-Butene	0.10	0.20	0.06	0.03	0.16
1-Butene	0.19	0.42	0.06	0.02	0.39
c-2-Butene	0.06	0.08	0.04	0.01	0.12
i-Pentane	0.82	0.71	0.60	0.25	1.62
n-Pentane	0.37	0.31	0.27	0.11	0.74
Isoprene	0.16	0.13	0.12	0.03	0.34
Benzene	0.98	0.89	0.66	0.19	2.40
Toluene	3.45	5.14	1.77	0.17	7.67
Ethyl-benzene	1.31	2.11	0.50	0.05	4.66
m, *p*-Xylene	0.73	1.25	0.17	0.03	2.81
o-Xylene	0.53	0.82	0.15	0.01	2.01
Furan	0.97	0.79	0.81	0.20	1.88
Acetonitrile	0.32	0.19	0.28	0.13	0.65
Acetaldehyde	3.36	2.62	2.66	0.86	7.63
Acetone/Propanal	4.16	2.57	3.58	1.51	8.27
Acetic acid	2.95	2.26	2.11	1.03	6.58
MVK/MACR	0.83	0.51	0.74	0.27	1.63
MEK/Butanal	1.09	1.08	0.70	0.30	2.62
BC	2.20	1.93	1.43	0.50	5.51
NO_2	7.79	11.90	2.50	0.29	27.59

ACPD
14, 30913–30945, 2014

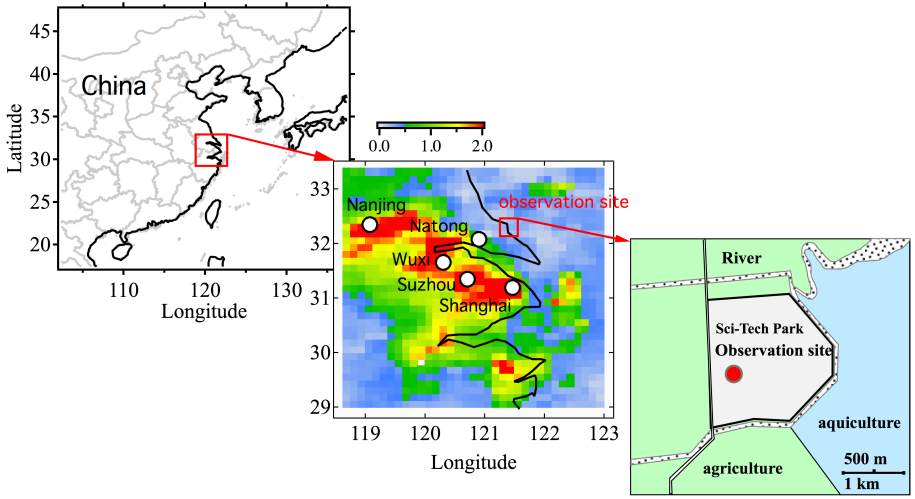

Figure 1. Geographic location of the observation site and the spatial distribution of monthly mean NO_x column density (unit: $\times 10^6$ molecule cm^{-2}, the data was from OMI observation, DOMINO version 2.0, http://www.temis.nl/airpollution/no2.html) during the field campaign period and the surrounding environment at the site.

ACPD
14, 30913–30945, 2014

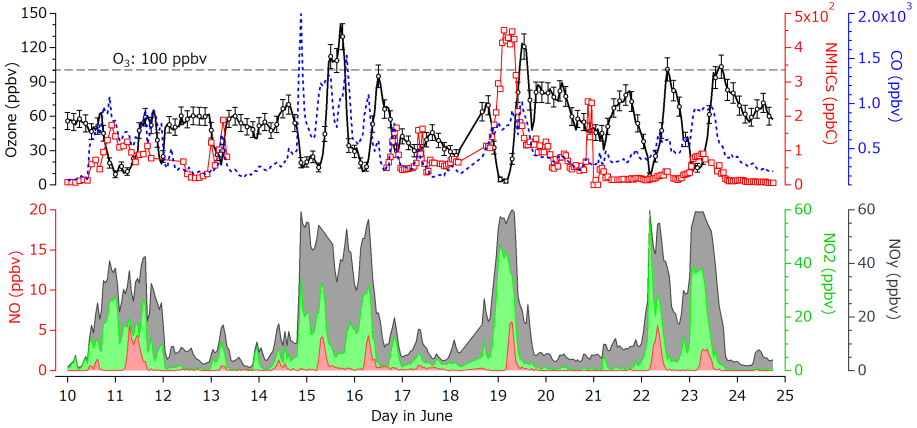

Figure 2. Time series of O_3, CO, NMHCs, NO, NO_2, and NO_y during the field campaign.

ACPD
14, 30913–30945, 2014

Major contributors and controlling factors of O_3 production in a rural Yangtze River Delta area

X. Pan et al.

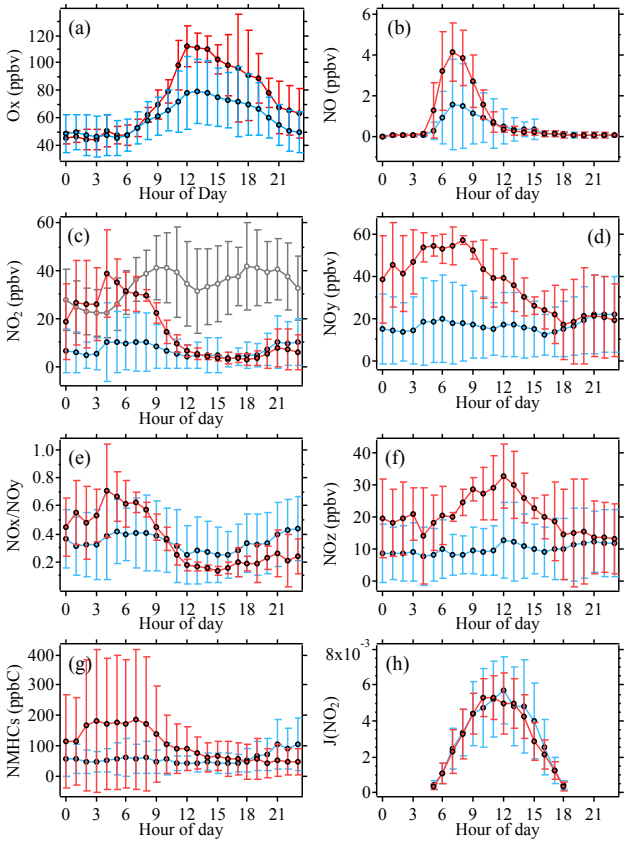

Figure 3. Diurnal variation in O_3, NO, NO_2, NO_y, NO_x/NO_y, NO_z, NMHCs, and $J(NO_2)$ during the field campaign. The blue and red colors represent the averaged diurnal patterns for the high-O_3 pollution (hourly O_3 mixing ratio > 100 ppbv even only once in a day) and low-O_3 pollution (hourly O_3 mixing ratio < 100 ppbv) days, respectively. The gray line in **(c)** indicates the NO_2 concentration in the downtown area of the Shanghai megacity.

ACPD
14, 30913–30945, 2014

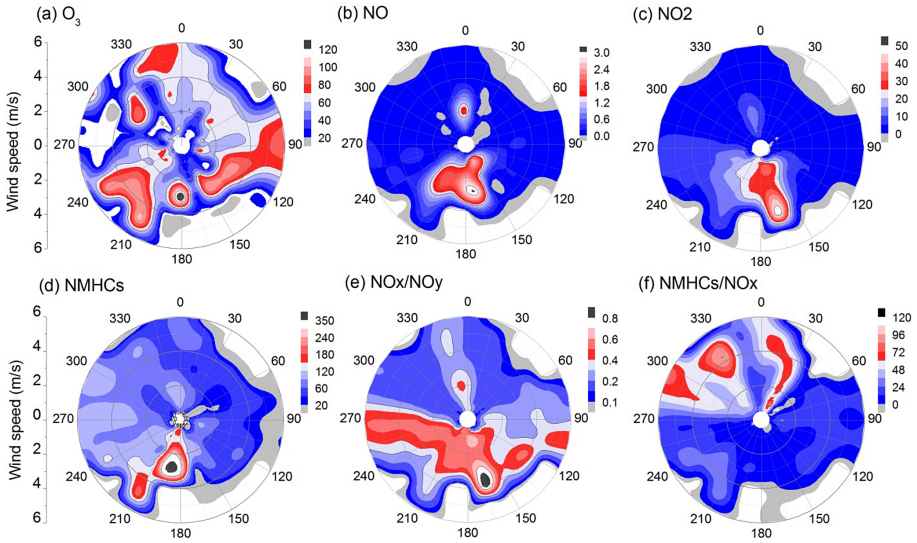

Figure 4. Dependence of the mixing ratios of O_3, NO, NO_2, NMHCs, NO_x/NO_y, and NMHCs/NO_x on wind direction and speed.

ACPD
14, 30913–30945, 2014

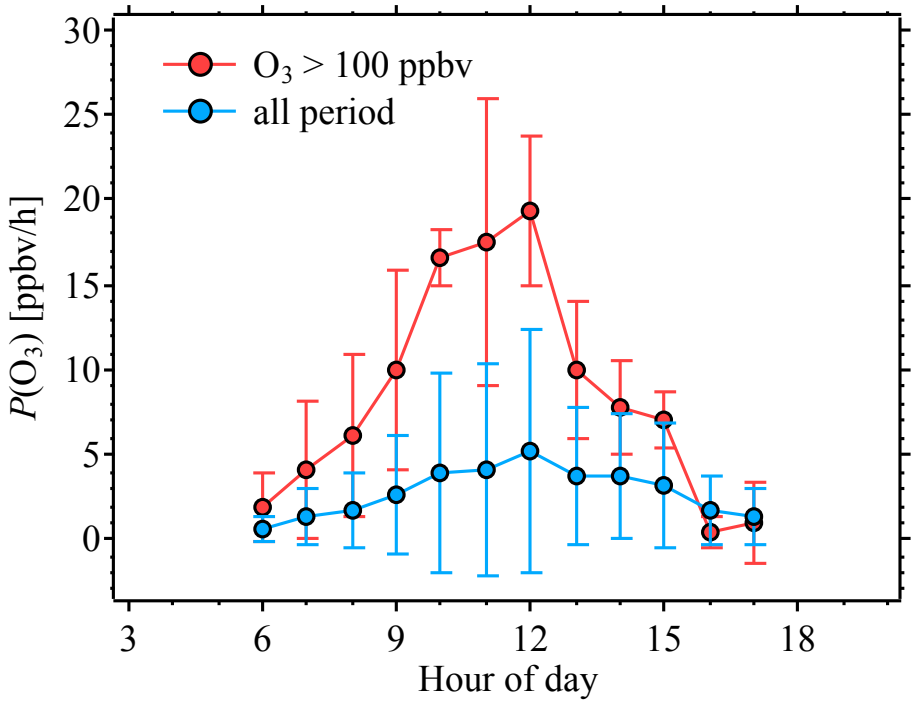

Figure 5. Diurnal variation in the net O_3 production rate for high-O_3 and low-O_3 pollution days

ACPD
14, 30913–30945, 2014

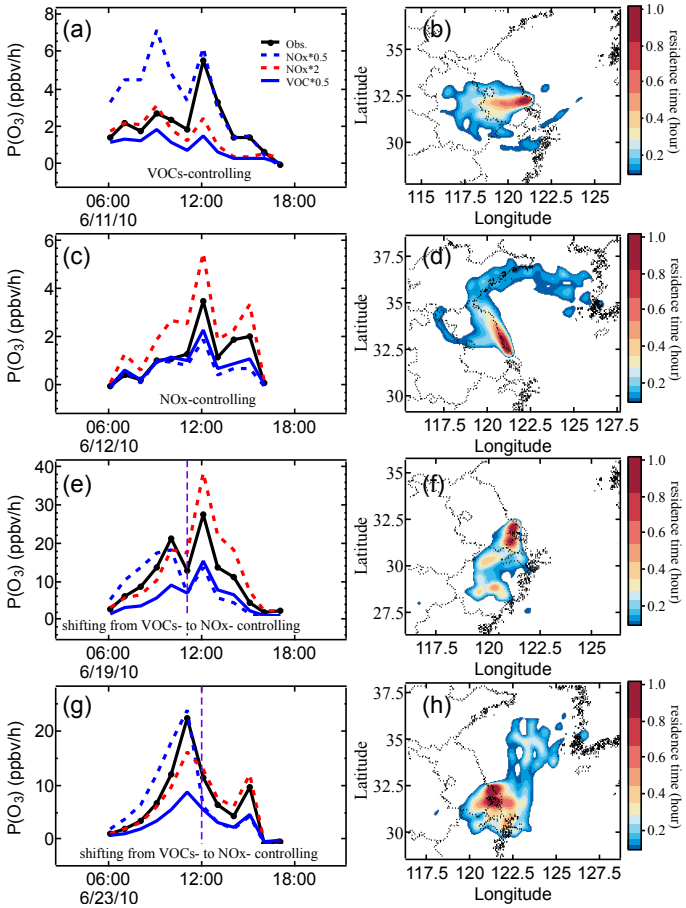

Figure 6. O_3 production sensitivity of the air masses with different footprint regions. The left panel shows the variation in O_3 production by artificial alteration of NO_x and VOCs; the right panel shows the footprint region for each case.

ACPD
14, 30913–30945, 2014

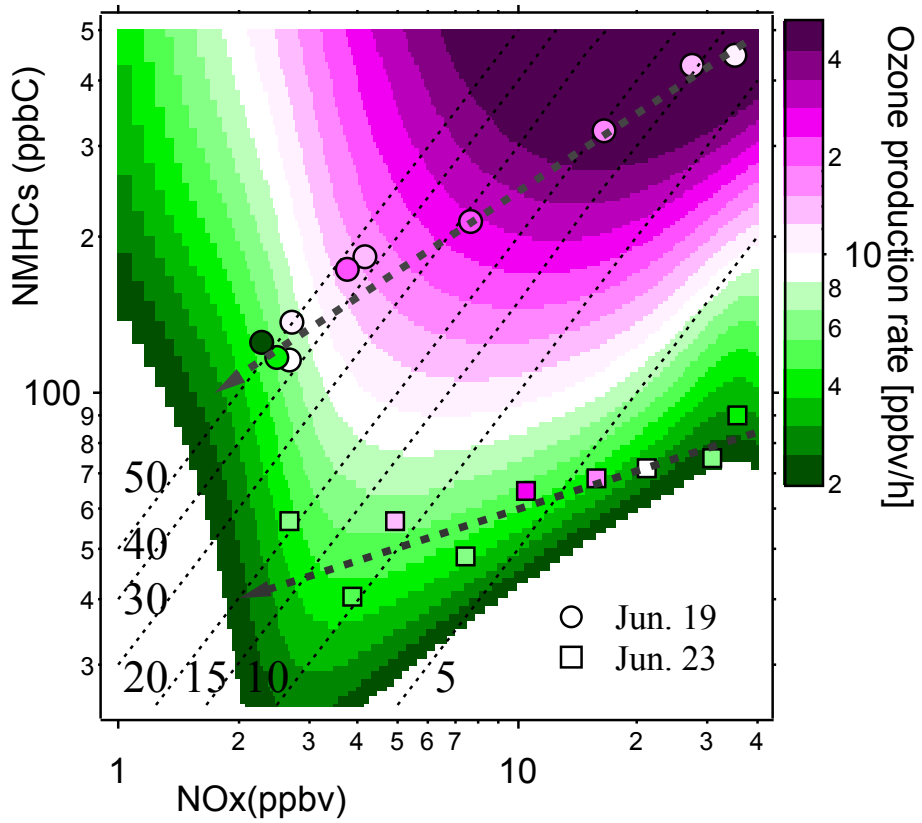

Figure 7. O_3 production isopleth plot derived from RACM sensitivity simulations at the observation site. The gray dashed lines indicate the direction of variation for the ambient NO_x concentration. The dot lines represent the trend of variation of NMHCs and NO_x.

ACPD
14, 30913–30945, 2014

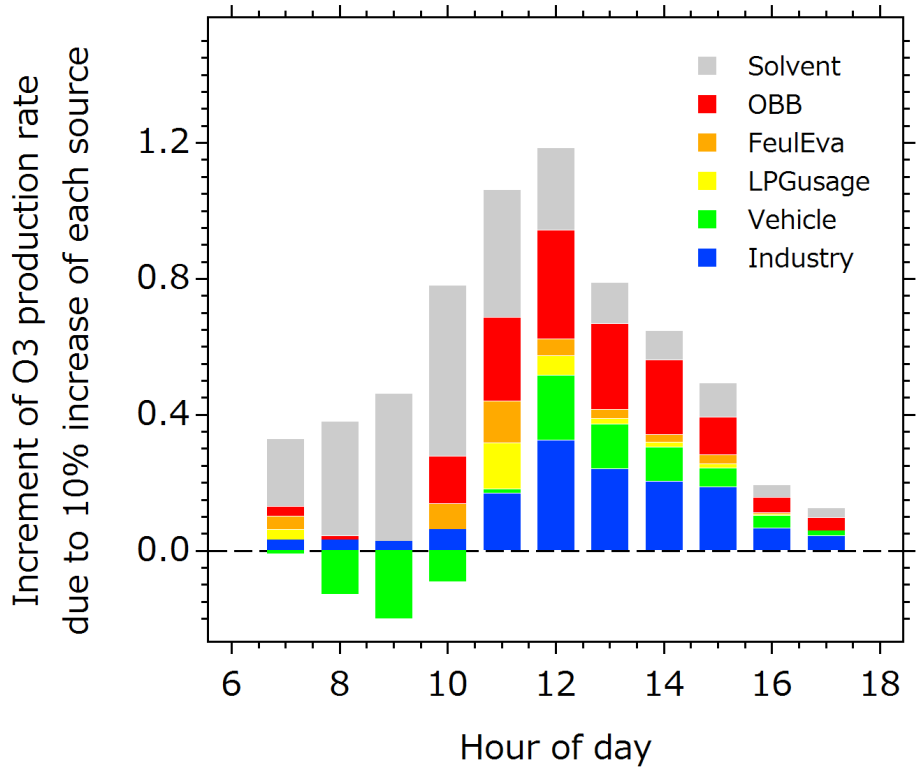

Figure 8. Diurnal variation in the sensitivity of each source to in situ O_3 production.

ACPD
14, 30913–30945, 2014